

Kinetic Monte Carlo simulations of the response of carbon nanotubes to electron irradiation

J. Kotakoski^{1,*}, A. V. Krasheninnikov^{1,2} and K. Nordlund¹

¹ Accelerator Laboratory, P.O. Box 43, FI-00014 University of Helsinki, Finland

² Laboratory of Physics, P.O. Box 1100, FI-02015 Helsinki University of Technology, Finland

(Dated: January 12, 2007)

Irradiation is increasingly used nowadays to tailor the mechanical and electronic properties of carbon nanotubes. As the complete understanding of the response of nanotubes to irradiation is still lacking, we have implemented the kinetic Monte Carlo method with Bortz-Kalos-Lebowitz-algorithm in a simulation code which enables modeling the behavior of irradiated nanotubes on macroscopic time scales. Within our model, the paths and energy barriers for the diffusion of irradiation-induced defects are obtained from density-functional-theory-based calculations. We have applied the model to single-walled nanotubes subjected to electron irradiation in a transmission electron microscope at different temperatures. In perfect agreement with the experiments, our simulations indicate that at temperatures higher than 300°C the annihilation of defects is efficient enough for almost perfect *in situ* self-healing of nanotubes. Our results on the irradiation doses needed to cut a single-walled nanotube with an electron beam are also similar to the experimental values. We also found that, surprisingly, for a certain range of relatively low temperatures (about 130–230°C) the temperature increase can have a negative effect on the self-healing.

Keywords: Kinetic Monte Carlo method, carbon nanotubes, defects, irradiation

*Electronic mail: kotakosk@acclab.helsinki.fi

PACS numbers:

I. INTRODUCTION

Controlled exposure of carbon nanotubes to energetic electrons and ions has been shown to enable tailoring many of their properties. The possibilities include engineering the atomic structure [1–6], altering the conductance [7] and elastic moduli [5] of nanotubes by creating defects or by doping with alien atom species [8–11], just to mention a few. Moreover, irradiated nanotubes can be used as masks against irradiation [12] and as nanoextruders via defect-mediated pressure build-up [13]. To fully exploit all the advantages of the irradiation-assisted engineering, a complete atomic-scale understanding of the response of nanotubes to irradiation is required.

Useful insights can be obtained from the data on the irradiation of bulk carbon systems such as graphite and diamond. However, many traditional concepts of irradiation physics are not directly applicable to nano-materials due to their inherent atomic-scale dimensions and a large number of surface atoms. The nano-scale results in a dissipation of the excess energy brought in by the impinging particle, which is different from that in bulk materials. The defect annealing may also proceed in a different way. For example, migration and annihilation of interstitials and vacancies in nanotubes, which govern the evolution of the nanotube morphology, are strongly affected by the nanotube geometry and irradiation conditions [14]. Understanding the evolution requires thus precise knowledge on the point defect migration and their interaction.

However, it is extremely difficult to obtain this knowledge experimentally, despite the recent advances [15, 16].

The most important and prolific defects in nanotubes which appear under irradiation are interstitials (adatoms), vacancies and their agglomerations [17]. The structure and energetics of atomic vacancies and vacancy clusters on carbon nanotubes have been studied at length [18–22]. The properties of single carbon adatoms and carbon dimers on nanotube walls have also been investigated [23, 24]. It was shown by density functional theory (DFT)-based methods that the migration of vacancies [21] and adatoms [23] depend on both the chirality and the diameter of the nanotube. However, due to computational limitations, these methods cannot be used to study the evolution of irradiated nanotubes at the experimental time scales (of the order of 1 – 10² seconds). Such time scale cannot be achieved even by molecular dynamics simulations with empirical potentials. Therefore, a statistical approach, such as kinetic Monte Carlo (KMC) method, has to be taken to study these phenomena at realistic system sizes and time scales.

In this work, we use the kinetic Monte Carlo method with the Bortz-Kalos-Lebowitz-algorithm to study the migration of irradiation-induced atomic vacancies and adatoms as well as defect annihilation and coalescence on single-walled carbon nanotubes with arbitrary chirality and curvature. We apply the method to nanotubes subjected to electron irradiation in a transmission electron microscope (TEM) at different temperatures. We show

that at temperatures above 300°C *in situ* annihilation of defects is fast enough for nearly perfect self-healing of nanotubes, in complete agreement with the experiments [6, 25]. Our results on the times needed to break a carbon nanotube with the electron beam in the TEM are also in line with the experiments [26]. Surprisingly, we further observe that an increase in the temperature can have a negative effect on the self-healing in a narrow temperature range above room temperature (about 130 – 230°C).

II. IMPLEMENTATION OF THE KINETIC MONTE CARLO METHOD FOR CARBON NANOTUBES

A. Atomic structure of carbon nanotubes

As usual in lattice KMC methods, we first create the underlying atomic lattice on which the migration of defects occurs. The atom coordinates for a nanotube are fully defined by the chiral indices [27]. Finite-size nanotubes are closed at the ends by caps formed by introducing a certain number of pentagons into the graphitic network. The shape of the cap depends on the tube diameter and chirality (in the simplest case this is just a hemisphere representing half of a fullerene). Within our method, the cap geometry is not explicitly taken into account. Instead we assume that the caps can be thought of as mirrors for migrating defects. Thus, whenever a defect enters a cap, its motion is reversed. This should be a reasonable approximation taking into account that no agglomeration of defects or amorphous carbon is found on tube caps even under extensive electron irradiation [26]. Open boundary conditions can also be used to model a segment of a much longer tube.

B. Basics of the kinetic Monte-Carlo method

The KMC method is an atomistic approach to simulate processes with known rates [28–30]. It is well suited to model atom migration, where the rates are given by a Boltzmann factor including a migration energy barrier. If the migration occurs in a step-by-step fashion by uncorrelated transitions, the KMC algorithm simulates the evolution of the system with a correct time scale [30]. Using the Boltzmann’s distribution function, the rate of occurrence for the migration steps, or any other activated phenomena, can be calculated with the equation

$$r_i = \nu_0 e^{-E_b^i/(k_B T)}, \quad (1)$$

where ν_0 is the typical frequency for the system in question, such as the vibration frequency of the lattice ($\nu_0 \approx 0.0037 \text{ fs}^{-1}$ for a carbon adatom on a nanotube [23]), E_b^i is the energy barrier for migration step i , k_B is Boltzmann’s constant and T is the temperature of the system.

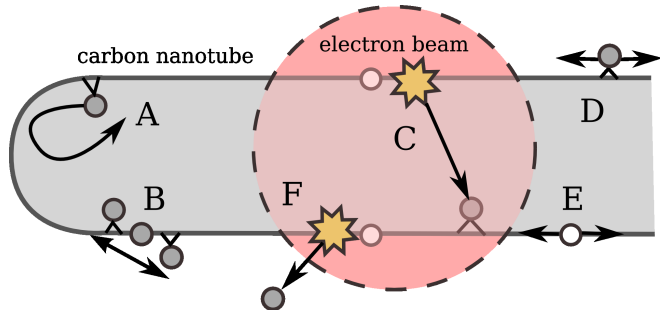


Figure 1: Schematic representation on the most important processes included in our model. (A) A diffusing endohedral adatom is reflected back from a cap. (B) Endohedral-exohedral transformation of an adatom through the exchange mechanism. (C) Electron impact creating a defect pair (white sphere - a vacancy, gray sphere - an adatom) by displacing a carbon atom. (D and E) Adatom and vacancy migration, respectively. (F) Creation of a vacancy by sputtering the displaced atom.

The phenomena which occur at a certain frequency ν_i independent of the temperature can be included by simply setting

$$r_i = \nu_i. \quad (2)$$

To efficiently model the time evolution of a defected nanotube, we have implemented the kinetic Monte Carlo method using the Bortz-Kalos-Lebowitz–algorithm [29]. The random numbers needed in the simulations are generated with the Mersenne Twister random number generator [31].

C. Defects, transitions and energy barriers

Within our approach, we addressed two types of defects: vacancies and adatoms (which play the role of interstitials in SWNTs [32]) and their agglomerations. The defects are located either on bonds between the carbon atoms (the lowest energy configuration for adatoms, both *endo-* and *exohedral*) or on atomic sites (vacancies). The reconstruction of the nanotube lattice due to defect agglomeration [22] is not taken into account at this stage. The allowed transitions (migration steps) for adatoms and vacancies are based on careful analysis of the density functional theory-based calculations [21, 23]. A schematic presentation of the processes involved in the simulations is given in Fig. 1.

The possible on-surface transition sites for an adatom are schematically presented in Fig. 2. In addition, the adatoms can also penetrate the nanotube wall by the exchange mechanism [33] (see Figs. 1 and 3). The same transition set with different energies are used for both endo- end exohedral adatoms, although the positions of the endohedral adatoms are in reality not exactly on top of the carbon-carbon bonds [23].

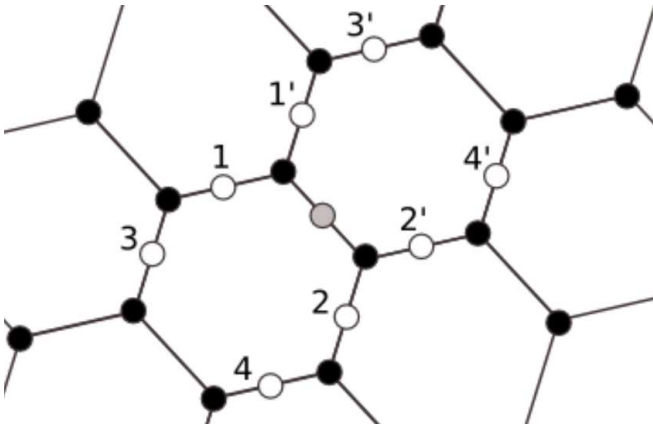


Figure 2: On-surface transitions for a carbon adatom on a single-walled carbon nanotube wall. Initial position of the adatom is marked with the gray dot, possible new locations with the white dots. The atoms in the underlying nanotube lattice are represented by the black dots.

To realistically model different types of on-surface transitions of the adatom, we have divided them first into short jumps (transitions $\{1, 1', 2, 2'\}$ in Fig. 2) and long jumps (transitions $\{3, 3', 4, 4'\}$). Both these categories are further divided into subsets depending on the orientation of the original bond with respect to the tube axis and the orientation of the bond on which the adatom is after the transition. The migration energy barriers for the on-surface transitions of adatoms on a SWNT with an arbitrary chirality are defined as

$$E_b = E_b^{GR}(\eta + \mu)^{(1-\beta)}, \quad (3)$$

where E_b^{GR} is the corresponding energy barrier for graphite,

$$\beta = \begin{cases} 1, & \text{if } r > r_{max} \\ 0, & \text{if } r < r_{min} \\ (r - r_{min})/(r_{max} - r_{min}), & \text{otherwise} \end{cases} \quad (4)$$

r_{min} is the radius of the smallest reasonable single-walled nanotube ($\sim 3.4 \text{ \AA}$) and r_{max} is the radius after which the curvature effect begins to vanish ($\sim 12.5 \text{ \AA}$, see *e.g.* reference [21]),

$$\eta = \begin{cases} E_b^{ZZ}/E_b^{GR}, & \text{if } E_b^{AC} > E_b^{ZZ} \\ E_b^{AC}/E_b^{GR}, & \text{otherwise,} \end{cases} \quad (5)$$

where E_b^{ZZ} and E_b^{AC} are the corresponding energy barriers for the smallest zigzag and armchair nanotubes, respectively, and

$$\mu = \begin{cases} \frac{E_b^{AC} - E_b^{ZZ}}{2E_b^{GR}}(1 + \sin(6\theta - \frac{\pi}{2})), & \text{if } E_b^{AC} > E_b^{ZZ} \\ \frac{E_b^{ZZ} - E_b^{AC}}{2E_b^{GR}}(1 + \cos(6\theta)), & \text{otherwise,} \end{cases} \quad (6)$$

where θ is the chiral angle of the nanotube.

Equation (3) can be used to estimate the energy barrier for any carbon nanotube from the known values for

graphite and small achiral nanotubes. Variable β takes into account the curvature effect whereas η and μ interpolate the energy barrier depending on the nanotube chirality. The equations have been chosen as a simple approximation which gives the correct results for the "limiting cases", that is armchair and zigzag nanotubes and, depending on the chiral angle, interpolate the data.

Our simulations [34] with the DFT-based tight-binding method [35] indicate that the best approximation for the energy barrier of adatom penetration through the nanotube wall by the exchange mechanism can be obtained using equation (3) with

$$\eta = 1 \quad \text{and} \quad \mu = 0 \quad (7)$$

for *exohedral* \rightarrow *endohedral* transition, and

$$\eta = \frac{\Delta E_b^{AC}}{E_b^{GR}} \quad (8)$$

and

$$\mu = \frac{\Delta E_{aa}^{ZZ} - \Delta E_{aa}^{AC}}{2E_b^{GR}}(1 + \cos(6\theta)), \quad (9)$$

for *endohedral* \rightarrow *exohedral* transition, where $E_b^{GR} \approx 1.25 \text{ eV}$ is the energy barrier for layer penetration for a carbon adatom on graphene as calculated by the DFT method [36], and ΔE_{aa}^{AC} and ΔE_{aa}^{ZZ} are energy differences between the exohedral and endohedral adatom configurations. These energy differences also depend on the orientation of the bond the defect is on for small armchair and zigzag nanotubes (see Fig. 3). All energies for graphite and small achiral nanotubes in equations (3–9) not given in the text can be obtained from reference [23]. In addition the more accurate data on endohedral adatom migration is listed in reference [14].

For vacancy migration, equation (3) can again be used, now with $\mu = 0$ and

$$\eta = \begin{cases} E_b^\perp/E_b^{GR}, & \text{for perpendicular transition,} \\ E_b^\parallel/E_b^{GR}, & \text{for parallel transition,} \end{cases} \quad (10)$$

where E_b^\perp and E_b^\parallel are now migration barriers for transitions of vacancies in small nanotubes in the perpendicular and parallel directions with respect to the tube axis, respectively. These energies can be obtained from reference [21].

We assume multi-vacancy formation whenever vacancies meet each other. As the migration barrier for a divacancy is around 5 eV, the multi-vacancies are set immobile. Also adatoms are allowed to agglomerate to form larger immobile clusters. However, this very seldom occurs within the simulations.

As a first approximation, whenever an adatom meets a vacancy with an odd number of neighbors (corresponding to a neighboring dangling bond), they annihilate, and are thus removed from the structure. To partially take into account the structure reconstruction, only two of every

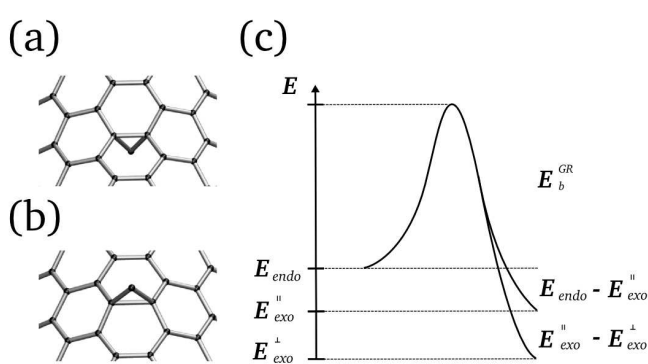


Figure 3: Adatom on a (10,10) SWNT above the bond oriented perpendicularly to the tube axis in the endohedral (a) and in the exohedral (b) configuration, and a schematic presentation on the energies related to the layer penetration process by the exchange mechanism for the adatoms (c). Note that the energy for the adatom in the endohedral configuration is practically independent of the orientation, and that the actual shape of the energy barrier is unknown, although the difference between the maximum value and E_{endo} is similar to the penetration energy barrier for adatoms on graphite.

three annihilations for a single vacancy and an adatom are accepted. In reality, however, the annihilation process is more complicated: some adatom–vacancy configurations result into a (5-7-7-5) Stone-Wales defect while others result into restoration of the perfect lattice [34]. As the energy barrier for transformation from the (5-7-7-5) defect to perfect lattice has been estimated to be very low when other adatoms are present [37], which is typically the case in irradiation experiments, neglecting this migration path can be assumed to have a significant effect on the results only at very low temperatures. Also curvature should in reality have a minor effect on the annihilation process. More detailed investigations on the annihilation of adatoms and vacancy-type defects are underway [34].

D. Practical implementation

The Monte Carlo method is implemented into a simulation code which allows one to model the behavior of SWNTs under irradiation. The simulations can be started with a certain number of defects introduced at random locations on the nanotube wall. To realistically simulate irradiation events, defects can also be created during the simulations according to a given displacement rate, corresponding to an experimental value. Also sputtering of atoms due to irradiation can be taken into account, and the characteristics of the electron beam, such as location and diameter, can be varied. The intensity of the irradiation is assumed to follow Gaussian distribution within the beam area.

While running the simulations, the code informs the user about simulation time, transitions, the total tran-

SWNT	θ	r (nm)	N_{at}
(8, 0)	0.00	0.31	75200
(6, 3)	12.37	0.31	74760
(5, 5)	30.00	0.34	81200
(10, 10)	30.00	0.68	162400
(18, 18)	30.00	1.22	292320

Table I: Single-walled nanotubes used in simulations, their chiral angles θ and radii r . N_{at} is the number of atoms in each simulated structure.

sition rate, and the numbers of different defects. Also the coordinates of the atoms and defects can be saved to make it possible to follow the evolution of the system as the simulation proceeds. The simulation ends when either the requested number of iteration steps is performed, the maximum simulation time, t_{MAX} , is exceeded, all rates in system equal to zero or the tube is destroyed.

III. SIMULATION RESULTS

As a test for our method, we applied it to various SWNTs with the aim to determine the temperature dependence of the concentration of point defects generated under electron irradiation in the TEM. The length of the simulated tubes was $1 \mu\text{m}$. The chiral indices, chiral angles θ and radii of the simulated nanotubes are given in Table I. The diameter of the electron beam was assumed to be 30 nm, and a displacement rate of 1 dpa/s was used. The tube was assumed to be a segment of a much longer tube, and hence open boundaries were used (defects vanish if they reach the end). In this work, we did not study the effect of caps which result in the reflection of the migrating defects. The role of caps will be addressed elsewhere [34].

To study the effect of the temperature on the defect concentration, we first simulated the behavior of a (10,10) SWNT under electron irradiation at several different temperatures. The adatom and vacancy concentrations as functions of time are presented in Fig. 4. Snapshots of an irradiated (10,10) SWNT are presented in Fig. 5 after 1, 2, 3, 4 and 5 seconds.

The defect concentration strongly depends on temperature. Note that defects are created during the whole simulation time. At low temperatures (≤ 525 K), the number of vacancies in the system increases rapidly leading to a break-up of the tube in less than ten seconds. The criterion for the break-up of the tube was that 20 % of the atoms in the area directly under the electron beam were missing. The choice of the criterion for the nanotube break-up was motivated by the experimental observations that in experiments the parts of the nanotube develop caps just before the break-up [26], which corresponds approximately to the loss of around 20% of atoms in the area where the structural changes are evident. Ac-

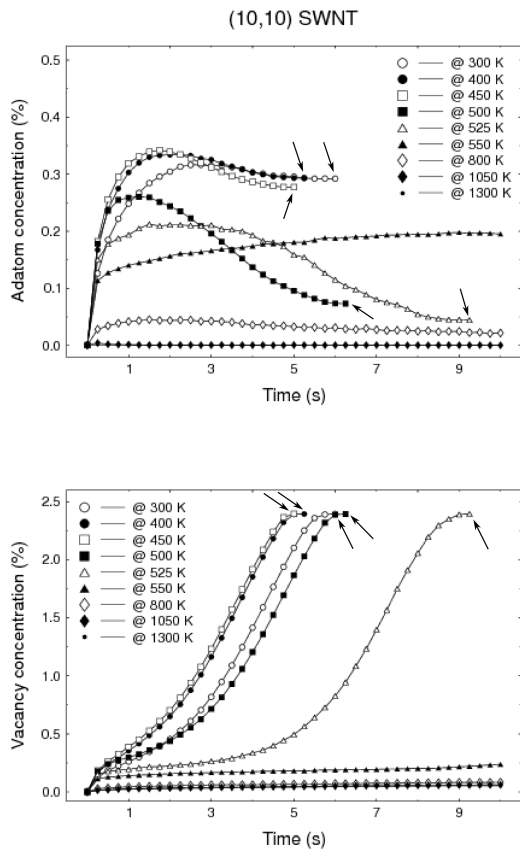


Figure 4: Adatom and vacancy concentrations in an irradiated (10,10) SWNT as a function of time at different temperatures. The arrows indicate the break-up points of the tubes. The presented data is averaged over several simulations (up to 40). The standard error is typically of the order of 10 % of the values. Note the macroscopic time scale of simulations.

According to Fig. 4, there is a temperature range slightly above room temperature ($\sim 130 - 230^\circ\text{C}$) at which the heating can surprisingly have a negative effect on the self-healing. This is most likely due to the increase in vacancy mobility making it easier for them to find each other and to form immobile multi-vacancy structures. However, only after about 300°C they are fast enough to escape the irradiated area to avoid rapid destruction of this part of the tube.

At experimental conditions quite similar to those used in the simulations, the time needed to break a nanotube at $600 - 700^\circ\text{C}$ was found to be around 5 s [26]. When these experiments are compared to our simulations, it has to be kept in mind that the tubes in the presented simulations are perfect at the beginning – no defects are introduced to the structures before the irradiation. In reality, however, even the highest purity carbon nanotubes contain at least one defect per every $4 \mu\text{m}$ [38] and most of the nanotubes used in the experiments are not of the highest quality. As was shown above, already ten seconds of irradiation of a (10,10) SWNT at 800 K leads to

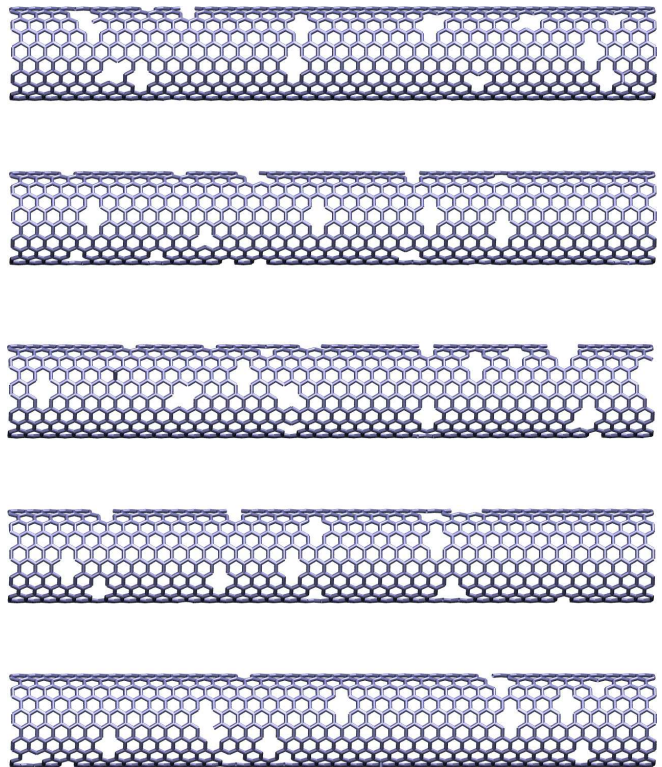


Figure 5: Snapshots of a part of a (10,10) SWNT irradiated at 800 K. The displacement rate is 1.0 dpa/s. Only the front side of a part of the irradiated area (10 nm-long) is shown. The length of the simulated structure was $1 \mu\text{m}$. The snapshots correspond to 1, 2, 3, 4 and 5 seconds of irradiation (from top to bottom). The defects are created during the whole simulation time, but the vacancy concentration increases very slowly due to efficient defect annealing.

approximately 0.1 % of vacancies in the structure. In the area in the middle of the electron beam the concentration is even higher.

According to our simulations, the effect of an initial vacancy concentration of 1 % shortens the cutting time needed to break a tube to 1/6 of the time for an undamaged one. Thereby it is no surprise that the cutting time for the perfect tubes is longer than the simulated 10 s at the higher temperatures. However, in a temperature range ($\sim 800 - 900^\circ\text{C}$) similar to the experiments presented in reference [26], the defect concentrations are seen to be increasing and are likely to lead to breakage with prolonged irradiation.

The reason for lower defect concentrations at temperatures $> 550 \text{ K}$ is the fact that at this temperature single vacancies become mobile. Indeed, the transition rate calculated from equation (1) for a migration energy barrier of 1.3 eV becomes at this temperature $\sim 5 \text{ s}^{-1}$, while at 525 K it is $\sim 1 \text{ s}^{-1}$ and at 500 K already $\sim 0.3 \text{ s}^{-1}$. Hence, at 550 K the vacancies can escape from the irradiated area before coalescing to larger immobile defects. Also the exohedral adatoms remain in practice immobile at temperatures lower than 500 K.

As each displacement creates one vacancy and one adatom (when we assume no sputtering), the concentrations of adatoms and vacancies are originally equal, then they change due to different migration rates. The account for sputtering increases the difference between adatom and vacancy concentration, which is particularly noticeable at low temperatures, Fig. 4. There is also a difference at 800 K. However, the reason is different – at higher temperatures the adatoms become fast enough to leave the structure. At temperatures above 1000 K essentially no adatoms remain in the tubes. As the endohedral adatoms are at these temperatures several orders of magnitude more mobile than the exohedral ones, they are also more likely to annihilate with the vacancies. Thereby the exohedral adatoms contribute more to the number of escaped defects.

To study the effect of diameter and chirality on the defect concentrations, we repeated the simulations at 800 K with four other SWNTs (see table I). The results of these simulations are presented in Fig. 6. Similar to the (10,10) SWNT, the difference in the vacancy and adatom concentrations can be seen for the (5,5) SWNT at 800 K. Interestingly, the third armchair tube studied, a (18,18) SWNT, seems to behave differently. The reason lies in the diameter of the tube - while it is harder for the adatoms and vacancies to meet each other in a larger structure, the adatoms escape the structure more easily, reducing the annihilation probability. The larger area decreases both the probability of the annihilation and the probability of the clustering. While the vacancies do not cluster, they will be distributed more evenly on the surface and will eventually escape or annihilate. Another reason is that there are fewer defects simply because the structure is larger but the beam diameter remains constant. Besides this, the difference between the number of escaped endohedral and exohedral adatoms vanishes as the tube diameter increases.

The concentration evolution depends not only on the diameter but also on the chirality of the tubes. When the tubes with similar diameter but different chiralities [i.e. (5,5) SWNT, (6,3) SWNT and (8,0) SWNT] are compared, the zigzag tube [(8,0) SWNT] is clearly the most stable against the irradiation. The values for the chiral (6,3) SWNT are in between the values for the armchair and zigzag tubes, as can be expected. The stability of the zigzag tubes is due to the somewhat lower migration energy barriers which ease the annihilation. The effect of chirality on vacancy concentration seems to be even higher than that of the temperature, although lower temperatures lead always to higher adatom concentration in the structure.

The displacement rate used in the simulations corresponds to a beam current of approximately 10^4 A/cm², which is much higher than the current usually used for TEM imaging (~ 1 A/cm²). However, the tubes can be broken by the beam even at low currents: a four orders of magnitude lower displacement rate leads to a breakage of a (10,10) SWNT on average after about ten seconds

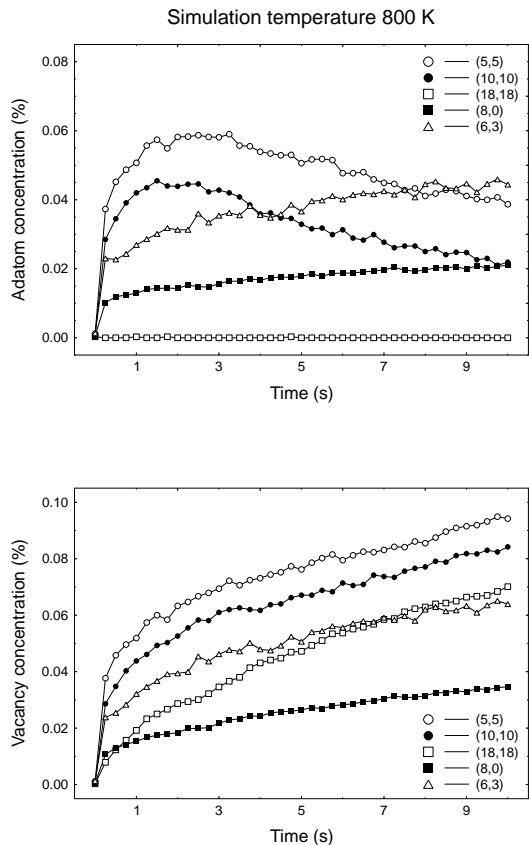


Figure 6: Adatom and vacancy concentrations in single-walled nanotubes with different chiralities as a function of time at 800 K. The presented data is averaged over several simulations (up to 40). The standard error is typically in the order of 10 % of the values.

at room temperature; only four seconds after the break-up with the higher displacement rate used in most of the simulations. The reason for the breakage is quite obvious; while the vacancies and exohedral adatoms are in practice immobile, it is only a matter of time when enough defects are created to break the tube. However, the results clearly show, in perfect agreement with experiments [6, 25], that temperatures higher than 300°C enable *in situ* annealing of the created defects if the beam current is low enough.

IV. CONCLUSIONS

In this article we have presented a model for simulating migration of point defects on carbon nanotubes. We have utilized the Bortz-Kalos-Lebowitz-algorithm [29] and used the migration paths and energy barriers obtained from density-functional-theory-based calculations to make the code both computationally effective and as accurate as possible. We have shown how this model can be used to study the temperature dependence of the re-

sponse of nanotubes to electron irradiation in the TEM at realistic time scales and with macroscopic system sizes.

Temperatures higher than 300°C were found, in perfect agreement with experiments [6, 25], to enable nearly perfect *in situ* annealing of the irradiation-induced defects, depending on the beam current. However, with a relatively high current ($\sim 10^4$ A/cm²) used in the simulations, the vacancy concentrations increase still after ten seconds of irradiation even at the highest studied temperatures. As the defect concentrations for irradiation temperatures above 300°C are significantly lower than at room temperature, the damage caused to the tubes in irradiation experiments can clearly be lowered by elevating the temperature.

Surprisingly, the highest defect concentration was found at temperatures in the range of 130–230°C. After ten seconds of irradiation at $\sim 530^\circ\text{C}$, vacancy concentration of about 0.1 % is found in a (10,10) SWNT. While 1 % of vacancies leads to a decrease of the time needed to break a tube to 1/6, this implies that differences in, for example, imaging time before the actual experiments can significantly alter the experimental results, although the simulated displacement rate was high as compared to the imaging conditions. Also the chirality of the nanotube was found to have a significant effect on the tube behavior under electron irradiation, further complicating the

comparison between different experiments. For example comparing the time needed to cut a nanotube with a TEM beam depends heavily on the pretreatment of the tube. However, our simulation results for the cutting times seem to be of the same order as the experimental values [26].

The introduced simulation code can at present be used in a wide variety of studies involving carbon nanotubes under/after ion and electron irradiation. It can also be applied to investigate the most important phenomena occurring during the growth of carbon nanotubes [39]. The implementation of more complex defect structures (such as reconstructed multi-vacancies [22, 40]), impurities [41] and the possibility to model the evolution of defected multi-walled carbon nanotubes [42] is underway.

Acknowledgments

The research was supported by the Academy of Finland under its Centers of Excellence Program. The authors would like to thank F. Banhart, Y. Gan and L. Sun for useful discussions. Grants of computer time at the Center for Scientific Computing, Espoo, Finland are gratefully acknowledged.

-
- [1] C.-H. Kiang, W. A. Goddard, R. Beyers, and D. S. Bethune, *J. Phys. Chem.* **100**, 3749 (1996).
 - [2] P. M. Ajayan, V. Ravikumar, and J.-C. Charlier, *Phys. Rev. Lett.* **81**, 1437 (1998).
 - [3] B. W. Smith and D. E. Luzzi, *J. Appl. Phys.* **90**, 3509 (2001).
 - [4] M. Terrones, F. Banhart, N. Grobert, J.-C. Charlier, H. Terrones, and P. M. Ajayan, *Phys. Rev. Lett.* **89**, 075505 (2002).
 - [5] A. Kis, G. Csányi, J.-P. Salvetat, T.-N. Lee, E. Couteau, A. J. Kulik, W. Benoit, J. Brugger, and L. Fórró, *Nat. Mat.* **3**, 153 (2004).
 - [6] F. Banhart, *Phil. Trans. R. Soc. Lond. A* **362**, 2205 (2004).
 - [7] G. Gómez-Navarro, P. J. De Pablo, J. Gómez-Herrero, B. Biel, F. J. Garcia-Vidal, A. Rubio, and F. Flores, *Nature Mater.* **4**, 534 (2005).
 - [8] G. H. Jeong, R. Hatakeyama, T. Hirata, K. Tohji, K. Motomiya, T. Yaguchi, and Y. Kawazoe, *Chem. Comm.* **1**, 152 (2003).
 - [9] J. Kotakoski, A. V. Krasheninnikov, Y. Ma, A. S. Foster, K. Nordlund, and R. M. Nieminen, *Phys. Rev. B* **71**, 205408 (2005).
 - [10] J. Kotakoski, A. V. Krasheninnikov, and K. Nordlund, *Nucl. Instr. and Meth. in Phys. Res. B* **240**, 810 (2005).
 - [11] C. Morant, J. Andrey, P. Prieto, D. Mendiola, J. M. Sanz, and E. Elizalde, *Phys. Stat. Sol.* **203**, 1069 (2006).
 - [12] A. V. Krasheninnikov, K. Nordlund, and J. Keinonen, *Appl. Phys. Lett.* **81**, 1101 (2002).
 - [13] L. Sun, F. Banhart, A. V. Krasheninnikov, J. A. Rodríguez-Manzo, M. Terrones, and P. M. Ajayan, *Science* **312**, 1199 (2006).
 - [14] F. Banhart, J. X. Li, and A. V. Krasheninnikov, *Phys. Rev. B* **71**, 241408(R) (2005).
 - [15] A. Hashimoto, K. Suenaga, A. Gloter, K. Urita, and S. Iijima, *Nature (London)* **430**, 870 (2004).
 - [16] K. Urita, K. Suenaga, T. Sugai, H. Shinohara, and S. Iijima, *Phys. Rev. Lett.* **94**, 155502 (2005).
 - [17] A. V. Krasheninnikov and K. Nordlund, *Nucl. Instr. and Meth. in Phys. Res. B* **216**, 355 (2004).
 - [18] A. J. Lu and B. C. Pan, *Phys. Rev. Lett.* **92**, 105504 (2004).
 - [19] J. Rossato, R. J. Baierle, A. Fazzio, and R. Mota, *Nano Letters* **5**, 197 (2005).
 - [20] S. Berber and A. Oshiyama, *Physica B* **376–377**, 272 (2006).
 - [21] A. V. Krasheninnikov, P. O. Lehtinen, A. S. Foster, and R. M. Nieminen, *Chem. Phys. Lett.* **418**, 132 (2006).
 - [22] J. Kotakoski, K. Nordlund, and A. V. Krasheninnikov, *Phys. Rev. B* **74**, 245420 (2006).
 - [23] A. V. Krasheninnikov, K. Nordlund, P. O. Lehtinen, A. S. Foster, A. Ayuela, and R. M. Nieminen, *Phys. Rev. B* **69**, 073402 (2004).
 - [24] M. Sternberg, L. A. Curtiss, D. M. Gruen, G. Kedziora, D. A. Horner, P. C. Redfern, and P. Zapol, *Phys. Rev. Lett.* **96**, 075506 (2006).
 - [25] O. Lehtinen *et al.*, unpublished.
 - [26] F. Banhart, J. X. Li, and M. Terrones, *Small* **1**, 953 (2005).
 - [27] M. S. Dresselhaus, G. Dresselhaus, and P. Avouris (Eds), *Carbon Nanotubes: Synthesis, Structure, Properties and Applications* (Springer, Berlin, 2001).

- [28] W. M. Young and E. W. Elcock, Proc. Phys. Soc. **89**, 735 (1966).
- [29] A. B. Bortz, M. H. Kalos, and J. L. Lebowitz, J. Comput. Phys. **17**, 10 (1975).
- [30] K. A. Fichtorn and W. H. Weinberg, J. Chem. Phys. **95**, 1090 (1991).
- [31] M. Matsumoto and T. Nishimura, ACM Trans. Mod. Comp. Sim. **8**, 3 (1998).
- [32] A. V. Krasheninnikov, K. Nordlund, and J. Keinonen, Phys. Rev. B **65**, 165423 (2002).
- [33] C. Xu, C.L.Fu, and D. Pedraza, Phys. Rev. B **48**, 13273 (1993).
- [34] J. Kotakoski *et al.*, unpublished.
- [35] T. Frauenheim, G. Seifert, M. Elstner, T. Niehaus, C. Köhler, M. Amkreutz, M. Sternberg, Z. Hajnal, A. Di Carlo, and S. Suhai, J. Phys.: Condens. Matter **14**, 3015 (2002).
- [36] Y. Ma *et al.*, unpublished.
- [37] C. P. Ewels, M. I. Heggie, and P. R. Briddon, Chem. Phys. Lett. **351**, 178 (2002).
- [38] Y. Fan, B. R. Goldsmith, and P. G. Collins, Nature Mater. **4**, 906 (2005).
- [39] K. Bolton, F. Ding, and A. Rosen, J. Nanosci. Nanotechnol. **6**, 1211 (2006).
- [40] M. Sammalkorpi, A. Krasheninnikov, A. Kuronen, K. Nordlund, and K. Kaski, Phys. Rev. B **70**, 245416 (2004).
- [41] T. Laponen, A. V. Krasheninnikov, M. Kaukonen, and R. M. Nieminen, Phys. Rev. B **74**, 073409 (2006).
- [42] M. Huhtala, A. V. Krasheninnikov, J. Aittoniemi, K. Nordlund, and K. Kaski, Phys. Rev. B **70**, 045404 (2004).